

Article

A Study of {10-12} Twinning Activity Associated with Stress State in Mg-3Al-1Zn Alloy during Compression

Boqin Lu¹, Wei Wang¹, Jinyi Yao¹, Liping Deng², Lei Xiao¹ and Bingshu Wang^{1,3,*} ¹ College of Materials Science and Engineering, Fuzhou University, Fuzhou 350108, China² School of Mechanical Engineering and Automation, Fuzhou University, Fuzhou 350108, China³ School of Advanced Manufacturing, Fuzhou University, Jinjiang 362200, China

* Correspondence: bswang@fzu.edu.cn

Abstract: An eight-sided prism sample, obtained from a hot-rolled AZ31 magnesium alloy sheet, was compressed at room temperature along the transverse direction to investigate the influence of local strain on twinning behavior using electron backscatter diffraction (EBSD) measurements, hardness distribution, and metallographic observations. The octagonal surface of the sample was divided into distinct regions based on hardness distribution and metallographic observations. Combined analysis of the Schmid factor (SF) and the strain compatibility factor (m') was employed to study twin variant selection. Basal on SF ratio distribution, the Schmid factor criterion, can predict over 75% of observed twin variants in regions A and D (normal stress samples). In contrast, 64% of twin variant selection behavior in region C (shear stress sample) can be effectively explained using a pure shear model. Twin variants with high strain compatibility factors may prefer activation to reduce stress concentration. The strain compatibility factor is more appropriate than the Schmid factor for analyzing the effect of local strain on the selection behavior of twin variants.

Keywords: AZ31 magnesium alloy; local strain state; twin variants selection; Schmid factor; strain compatibility factor



Citation: Lu, B.; Wang, W.; Yao, J.; Deng, L.; Xiao, L.; Wang, B. A Study of {10-12} Twinning Activity Associated with Stress State in Mg-3Al-1Zn Alloy during Compression. *Metals* **2024**, *14*, 502. <https://doi.org/10.3390/met14050502>

Academic Editors: Marcello Cabibbo and Roberto Figueiredo

Received: 15 February 2024

Revised: 17 April 2024

Accepted: 23 April 2024

Published: 25 April 2024



Copyright: © 2024 by the authors. Licensee MDPI, Basel, Switzerland. This article is an open access article distributed under the terms and conditions of the Creative Commons Attribution (CC BY) license (<https://creativecommons.org/licenses/by/4.0/>).

1. Introduction

Magnesium alloys have low density, high specific strength, and excellent properties such as high durability, high absorption, excellent electrical and thermal conductivity, and outstanding electromagnetic shielding and damping properties [1,2]. As the lightest structural metal, magnesium alloys have broad application prospects in aerospace, biomedicine, and electronics [2–4]. Twinning plays an important role in the low-temperature deformation of magnesium alloys [5–7]. Moreover, the incidence of {10-12} twinning is closely related to the initial crystal orientations and the loading path [8–11]. {10-12} $\langle -1011 \rangle$ can be aroused by extension stress along the c -axes, which is favorable during parallel to c -axes tension or perpendicular to c -axes compression [12–15]. Theoretically, Mg alloy has six equivalent {10-12} twin variants within each grain. Several studies have investigated variant selection using a Schmid factor criterion [16–18]. A previous study by Hong et al. [16] indicated that the activation of {10-12} twinning depends on strain paths, and the selection mechanism of the six variants was governed by the Schmid factor (SF) criterion. Song et al. [17] suggested that variant selection in twinned grains generally follows the Schmid factor criterion. Various non-Schmid phenomena have been recorded, attributed to the different local stress from externally applied stress [19–21]. Lou et al. [22] suggested that non-Schmid behavior in certain grains is linked to local stress variations near the grain boundary, resulting from strain accommodation between grains.

Several recent publications [17,23–25] aim to understand the strain accommodation necessary for twinning to spread across grain boundaries. Intragranular multiple twin variants frequently occur and are conducive to the formation of twin–twin structures

to continuously coordinate the further deformation. Twin–twin interactions affect subsequent twinning and the division and refinement of grains, leading to twin-induced hardening [26–28]. The quantification of strain accommodation can be assessed using a geometric compatibility factor, $m' = \cos(\Psi) \cdot \cos(\kappa)$, where Ψ and κ represent the angles between the normal of the twinning plane and the twinning shear direction of adjacent grains, respectively. Guo et al. [29] conducted a thorough analysis of the SF criterion and local strain accommodation to study the variant selection of {10-12} twinning. The researchers found that stress concentration relief happened through transfer across grain boundaries and the formation of new twinning. Shi et al. [30] also studied cross-grain boundary contraction paired twins (CTWs) and found that the formation of CTWs was influenced by the twinning shear compatibility across grain boundaries, characterized by a high m' value. The statistical results showed that macro stress near the grain boundary significantly influenced the stress state, leading to twinning initiation. The presence of non-Schmid twin variants indicates that strain compatibility in neighboring grains significantly influences variant selection.

The local strain state can also have an impact on the selection of twinning variants. Currently, few studies have examined the impact of the local strain state on twinning variant selection [31–33]. Huang et al. [32] analyzed twinning variant selection behavior in different local strain areas and observed the complexity of twinning behaviors. In regions with significant shear strain, the presence of twin variants can be explained by the Schmid factor criterion, which involves assessing the local stress state as a pure shear model. The impact of local strain on the strain compatibility of cross-boundary twin pairs is not yet fully understood.

The primary aim of this study is to investigate how local strain affects {10-12} twinning behavior in Mg-3Al-1Zn alloy under compression. In order to produce inhomogeneous localized strains after compression, an octahedral prism sample was used. The Schmid factor, strain compatibility factor, and twinning strain tensor were calculated using the results of electron backscattered diffraction (EBSD) to study the selection of twinning variants.

2. Materials and Methods

In the present study, the as-received material was a commercial hot-rolled AZ31 (Mg-3%Al-1%Zn) magnesium alloy sheet. Specimens were annealed at 530 °C for 1 h. The observation shows that the material exhibits a strong {0001} basal texture and a twin-free equiaxed grain structure, with an average grain size of ~35 μm, as shown in Figure 1. An eight-sided prism with bottom sides and edge sides measuring 8 mm each was obtained from the as-received material. Specimens were compressed at a strain rate of 0.01 s⁻¹ and a final strain of 3.9%, with the loading direction (LD) aligned parallel to the transverse direction (TD).

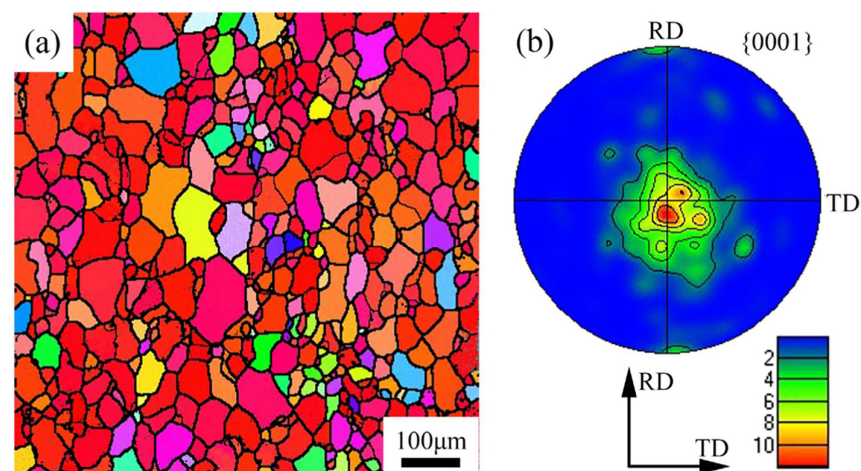


Figure 1. The as-received AZ31 Mg alloy sheet: (a) Orientation map and (b) {0001} pole figure.

The hardness was measured at 0.5 mm intervals along lines a to e. Microstructure and texture observations were made in areas A–D after the compression (see Figure 2b). The specimens were electrolytic polished for 90 s in a Struers ACII electrolyte solution at $-5\text{ }^{\circ}\text{C}$ and 20 V. The electron backscatter diffraction (EBSD) observations were conducted using a Zeiss Supra 55 FEG-SEM (Jena, Germany) and twinning behaviors were analyzed using HKL channel 5 software.

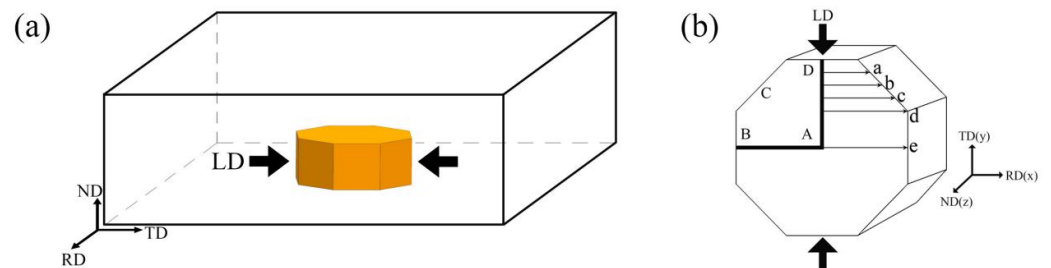


Figure 2. (a) Schematic illustration of the sample (RD, TD, and ND represent the rolling, transverse, and normal directions of the rolled sheet, respectively; LD represents the loading directions). The lengths of both the bottom and edge sides are each 8 mm. (b) Schematic illustration of hardness test and texture observation.

3. Results and Discussion

3.1. Distribution of the Hardness Values

The distribution of hardness values along the five lines is shown in Figure 3a. Because of the symmetry of the sample, only a quarter of the octagonal surface was measured. The decrease in hardness values from line a to line e is evident, which can be attributed to the different deformation mechanisms. In addition, the hardness values decrease as the tested position moves away from the center for each line. The equivalent plastic strain E_{yy} distribution obtained via the finite element simulation is shown in Figure 3b. The relevant parameters of AZ31 magnesium alloy used in the simulation calculation were as follows: the elastic modulus E was 44.8 GPa; the Poisson's ratio was 0.35; the deformation temperature was room temperature; the deformation rate was 0.001 s^{-1} ; and the amount of deformation was 4%. It can be found that the hardness values and the strain are positively correlated on the whole. The variation in hardness at different positions suggests non-uniformity in the local strain state, which could affect twinning activation.

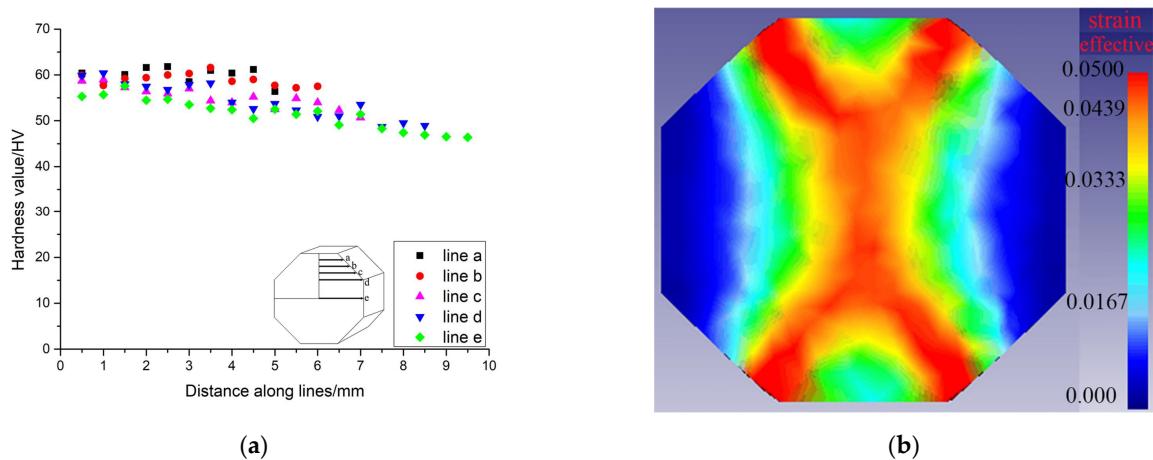


Figure 3. (a) Hardness values measured along lines of the eight-sided prism sample. (b) The equivalent plastic strain E_{yy} distribution via finite element simulation following compression.

3.2. Microstructure after Uniaxial Compression

To investigate the effect of local strain on the microstructure, the octagonal surface is divided into nine areas labeled as letters a–i. A large number of differences are denoted in the regions a–i, as shown in Figure 4. It can be seen that the twinning volume fraction is higher in the center areas (b, e, and h), followed by the corner areas (a, c, g, and i), and then the side areas (d and f). The grain sizes significantly decreased in the center regions compared to those in other regions. It is worth noting that a more localized strain exists in the central regions, and this result is explained in detail in the next section.

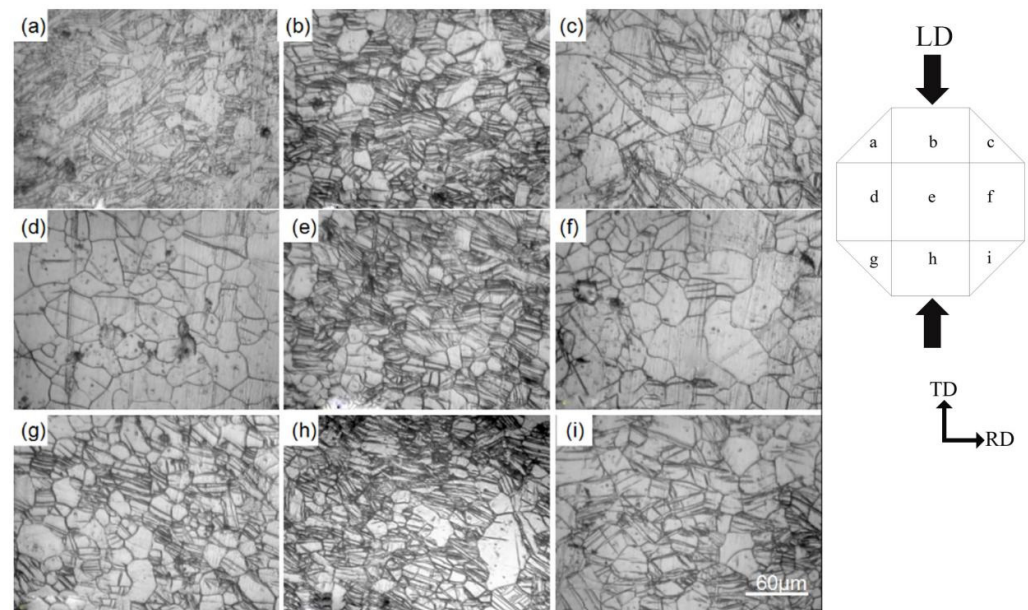


Figure 4. Optical micrographs at different areas of the sample after $\epsilon = 3.9\%$ compression at room temperature. (a) region A, (b) region B, (c) region C, (d) region D, (e) region E, (f) region F, (g) region G, (h) region H, (i) region I.

3.3. Microstructure and Texture Differences in Different Regions

Figure 5 shows the orientation image maps, grain boundaries maps, and $\{0001\}$ pole figures of four regions. Red lines represent $\{10\text{-}12\}$ extension twinning boundaries. It can be seen that twinning is significantly present in regions A, C, and D, while region B shows minimal to no twinning. This may be due to the fact that region A and region D experienced direct compression from the force, resulting in normal strain with minimal local shear strain [34], while region C experienced both normal and shear strain. In addition, region B was located outside the directly compressed area, which hindered twinning activation due to the low normal strain. From the $\{0001\}$ pole figures, it is evident that the matrix orientations are centrally distributed around the ND, while the variant orientations rotate 86.4° after compression. The distinction is based on the different orientations of variants in region A and region D, which rotate to the TD (y), while variant orientations in region C deviate by approximately 45° between the TD (y) and RD (x), referred to as the xy-direction for ease of reference. From the above analysis, it can be seen that the twinning orientations rotate to different regions due to the non-uniformity of the stresses.

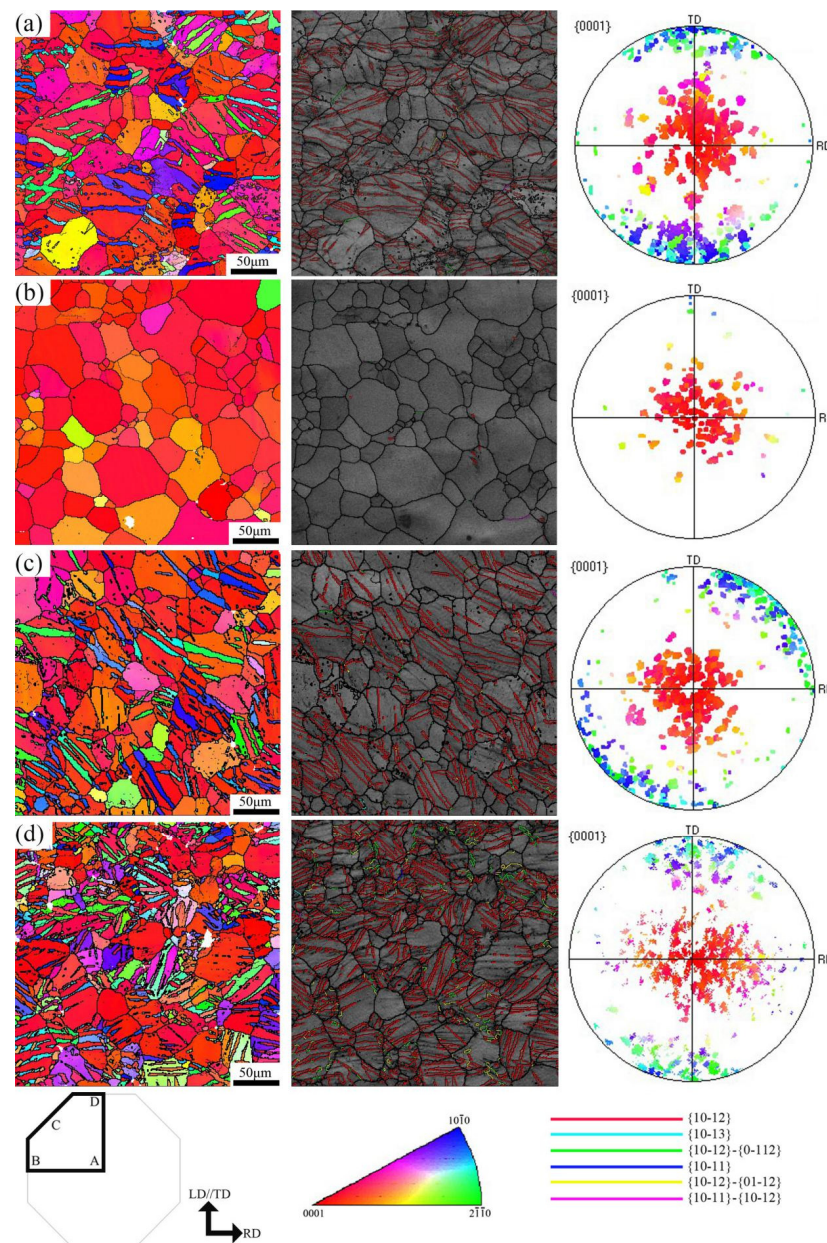


Figure 5. Orientation image maps, grain boundaries maps, and {0001} pole figures of four regions: (a) region A; (b) region B; (c) region C; and (d) region D.

3.4. SF Ratio Distribution

The formula $SF = \cos(\lambda) \cdot \cos(\varphi)$, where $\lambda(\varphi)$ is the angle between the loading direction and the normal to the twinning plane, was used to obtain the Schmid factors for twinning [35]. An improved SF_{ratio} has been proposed based on global SF analysis. The SF_{ratio} is defined as the SF value of the activated twin variant divided by the maximum SF value. For each grain analyzed, the SFs for all six potential twin variants were calculated.

For a thorough examination of the twin variant selection behavior using the SF criterion, a total of 97 grains with 123 twin variants in region A, 102 grains with 129 twin variants in region C, and 143 grains with 191 twin variants in region D were selected. The distributions of SF_{ratio} values for regions A, C, and D are shown in Figure 6. It can be seen that about 45% of the variants in region A (Figure 6a) have the highest SF ($SF_{ratio} = 1$), while roughly 30% of the other variants have the second-highest SF ($0.9 < SF_{ratio} < 1$). In region D (Figure 6b), about 43% of the variants have the highest SF, while approximately 35% have the second-highest SF. From the above analysis, most of the twin variant selection

mechanisms obey the Schmid factor law. By contrast, region C experiences both normal and shear stresses and leads to an indeterminate stress state. Huang et al. [32] also reported a similar situation and suggested a pure shear model similar to the rolling model. Therefore, it is possible to create a stress state model that combines tension and compression. The SF values can be recalculated using the equation $SF = (\cos\lambda_1 \cdot \cos\varphi_1 - \cos\lambda_2 \cdot \cos\varphi_2)/2$, where λ_1 (φ_1) represents the angle between the tensile stress direction and the twinning plane normal (twinning plane), and λ_2 (φ_2) represents the angle between the compressed stress direction and the twinning plane normal. The distribution of SF_{ratio} values for region C under this stress state is shown in Figure 6c. Around 22% of twin variants exhibit the highest SF values, while over 42% of twin variants show the second highest SF values. The data suggest that the SF values for region C do not satisfy the Schmid factor criterion well.

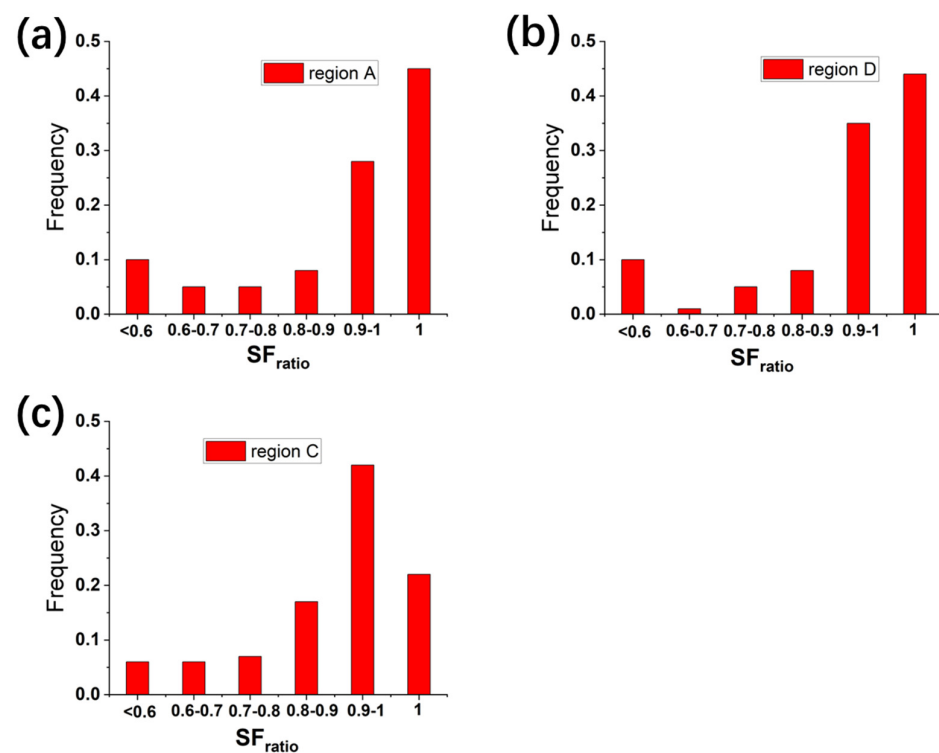


Figure 6. Frequency of twin variants displayed in terms of SF_{ratio} using an assumption of uniaxial loading: (a) 123 twin variants in region A, (b) 191 twin variants in region D, and (c) 129 twin variants in region C.

3.5. Strain Compatibility Factor

The lamella connecting two adjacent grains is termed “paired twins”, while the lamella connecting three or more neighboring grains is referred to as twin chains. The accurate prediction of the activated twin variant in deformed Mg alloy using only the SF can be quite challenging [36,37]. Thus, strain compatibility factor m' is used to study the selection behavior of twin variants in the presence of the inhomogeneous local strain. The m' ratio is defined as the ratio of the m' of the activated twin variant to the highest m' of the twin variant. Figure 7 illustrates the distribution of the rank, value, and ratio of m' for the three regions. There are 49 twin variants in region A, 62 twin variants in region C, and 55 twin variants in region D. In all three regions, the occurrence of the twin variant with a rank of 1 for paired twins is over 70%, whereas that for twin chains exceeds 80%, as shown in Figure 7a–c. It can be suggested that strain compatibility factor m' is more appropriate than the Schmid factor for analyzing the twin variant selection. Additionally, about 60% of twin variants in both paired twins and twin chains exhibit high m' values (>0.8), as shown in Figure 7d–f. It is interesting to note that the results of the m' ratio distribution closely resemble those of the m' rank distribution. The percentage of the twin variant with

a m' ratio of 1 for paired twins is over 70%, while those for twin chains is about 80%, as seen in Figure 7g–i. This means that the strain compatibility factor may not be affected by the direction of the force. More importantly, for all specimens, the general rule is that the selection behavior of most of the {10-12} twinning variants is influenced by the strain compatibility factor in scenarios with inhomogeneous local strain.

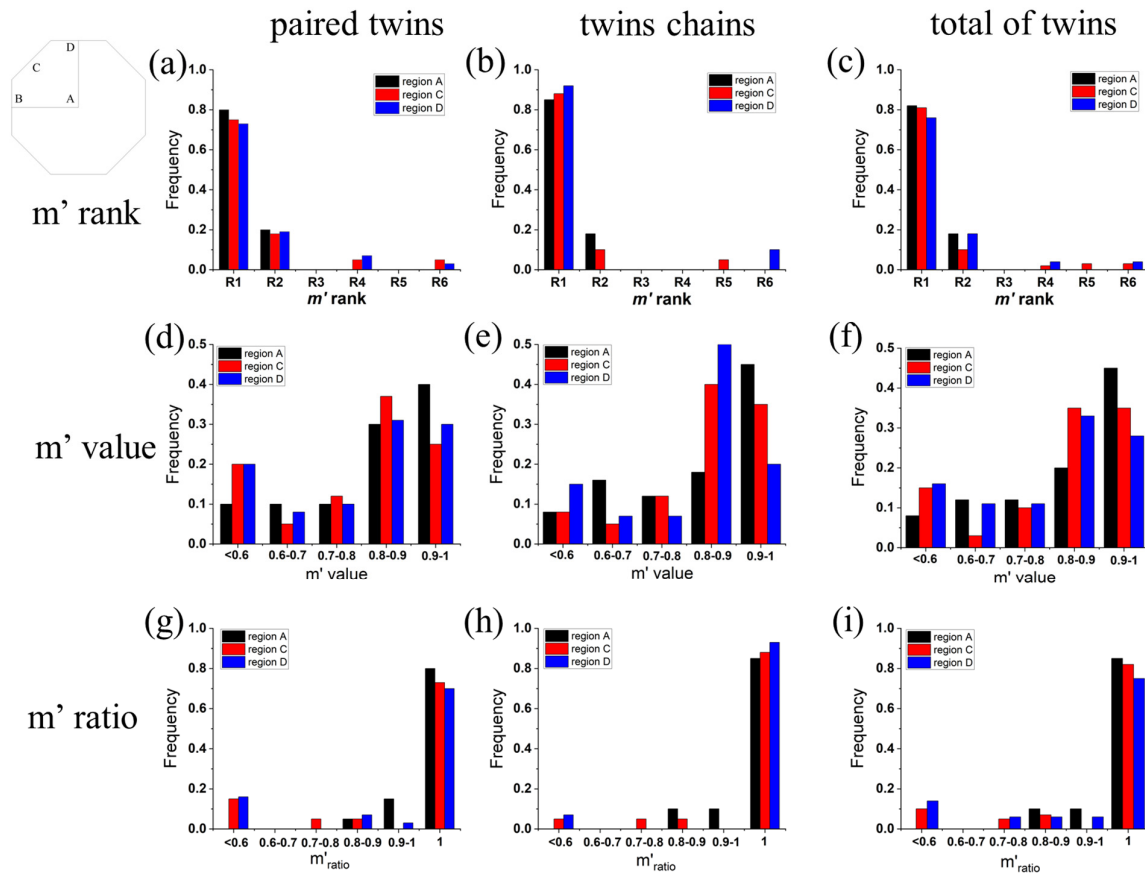


Figure 7. Distribution of m' rank, m' value, and m' ratio of the observed paired twins (a,d,g), twin chains (b,e,h), and all twin variants (c,f,i) for the three regions.

3.6. Twin Chains in Different Regions

In this research, the twin–twin interactions occur in specimens. It is known that deformation twins are formed in accordance with external stress, aided by the concentrated stress due to dislocation pile-up [33]. Thus, what would happen if twinning variants meet? Figure 8a illustrates a twin chain T_{h1} - T_i - T_j across three neighboring grains in region A. The specific characteristics of six potential twin variants V1–V6 of the parent grain M_h , M_i , and M_j are depicted in Figure 8b. It can be seen that variants T_{h1} , T_i , and T_j all exhibit the second-highest SFs, which are very close to the highest SFs. The distribution of the strain compatibility factor m' for the twin chain is displayed in Figure 8c. The strain compatibility factor m' exhibits its highest value of 0.966 between T_i and T_{h1} and also records the highest value of 0.937 between T_i and T_j . In order to investigate the relationship between the activated twin variants and the local strain state, the strain tensors of all the activated twin variants were calculated using the method described by Luo et al. [18]. To reveal the role of these twins, the twin strain tensors for T_{h1} , T_i , and T_j are illustrated in Figure 8d. For the region A, the compression direction is y-direction. Thus, the values of ϵ_{yy} are negative. The absolute value of ϵ_{yy} is significantly larger than zero, which suggests that it can coordinate the strain along the compression axis [38]. In addition, the values of ϵ_{xx} are positive when there is an extension strain component along the x-direction. For region A, the activation of

the twin chain is essential for facilitating compressed deformation in the force direction, influenced by a combination of the Schmid factor criterion and strain accommodation.

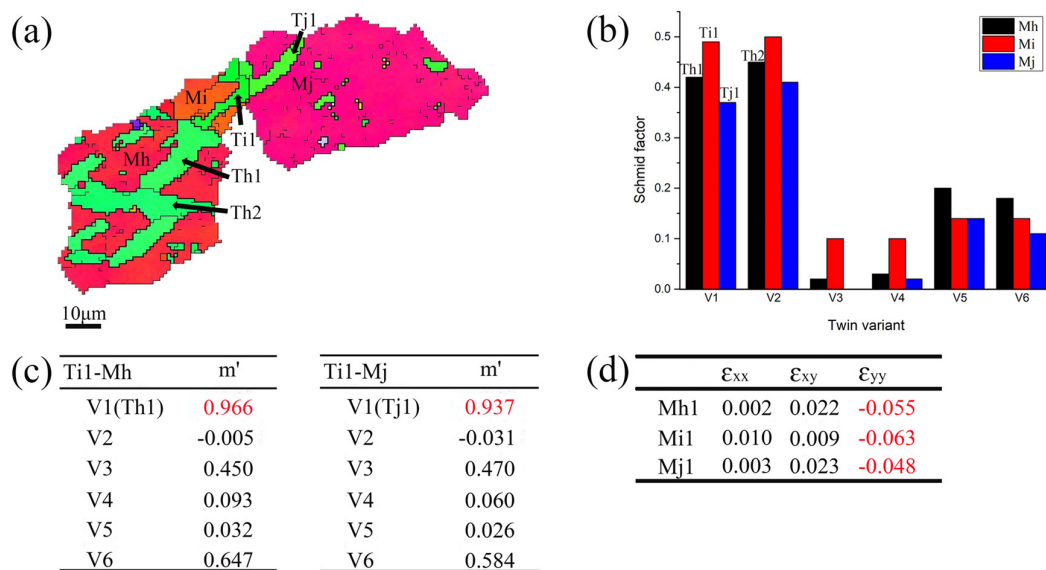


Figure 8. Analysis of twin chain across three neighboring grains, which follow Schmid factor law and strain compatibility factor law for region A: (a) EBSD map; (b) Schmid factor distribution figure; (c) m' distribution figure; and (d) strain tensors for twin variants.

For region C, the stress state is relatively complex. Figure 9a illustrates a twin chain T_{k1} - T_l - T_{n1} spanning three adjacent grains in region C. In this study, the distribution of SF is calculated using the pure shear model for region C. It can be seen that the SF values are significantly lower than 0.5 (Figure 9b). The twinning SF for T_{k1} is the second highest, for T_l it is the fifth highest, and for T_{n1} it is the third highest, respectively. The results indicate that the activation of twin variants is not influenced by the Schmid factor criterion. Figure 9c illustrates that the strain compatibility factor m' is highest between T_l and T_{k1} (0.801) and also highest between T_l and T_{n1} (0.895). This twin chain activation indicates the effect of strain accommodation, which is independent of the force direction. It is reported that the induced internal stresses, when accommodation is easy, are small and even low macroscopic SFs are sufficient to form twins [39,40]. Here, strain accommodation in neighbor grains can clarify this low SF variant activation. Figure 9d illustrates the twin strain tensors of T_{k1} , T_l , and T_{n1} . It can be seen that the absolute value of ϵ_{xy} is significantly larger than zero, which suggests that it can coordinate the strain along the xy-direction. Consequently, the twin variant possessing the highest m' rank is favored for activation in the form of a twin chain to release the local stress concentration.

Figure 10a illustrates another twin chain T_{r1} - T_{s1} - T_t across three adjacent grains in region C. The SF values of variants T_{r1} , T_{s1} , and T_t are all significantly less than 0.5, as shown in Figure 10b. The twinning SF for T_{r1} is the fifth highest, for T_{s1} it is the fourth highest, and for T_t it is the third highest, respectively. It can be seen that the activation of twin variants is not influenced by the Schmid factor criterion. Figure 10c illustrates that the strain compatibility factor m' between T_{s1} and T_t is the highest (0.823), whereas the factor between T_{s1} and T_{r1} is the fifth highest (-0.001). This observation suggests that the activated twin chain does not conform to the law of strain accommodation. The twin strain tensors of T_{r1} , T_{s1} , and T_t mainly coordinate the strain along the y-direction, which indicates that the twin chain experiences compressed deformation in the y-direction rather than the xy-direction, as shown in Figure 10d. This indicates that the generation of certain paired twins cannot be explained by the strain compatibility factor or Schmid factor.

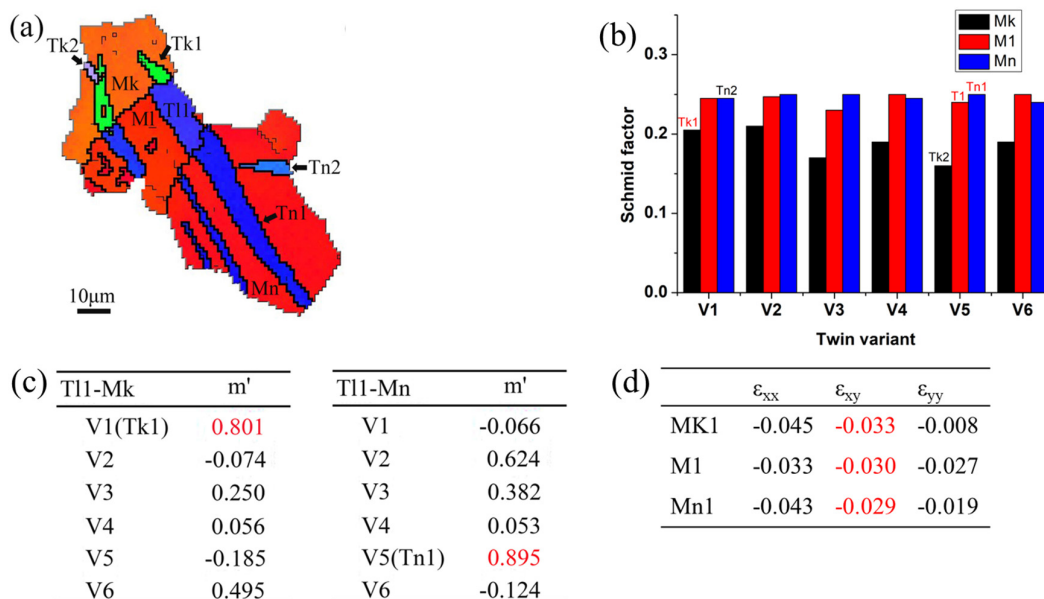


Figure 9. Analysis of twin chain across three neighboring grains, which follow strain compatibility factor law for region C: (a) EBSD map; (b) Schmid factor distribution figure; (c) m' distribution figure; (d) and strain tensors for twin variants.

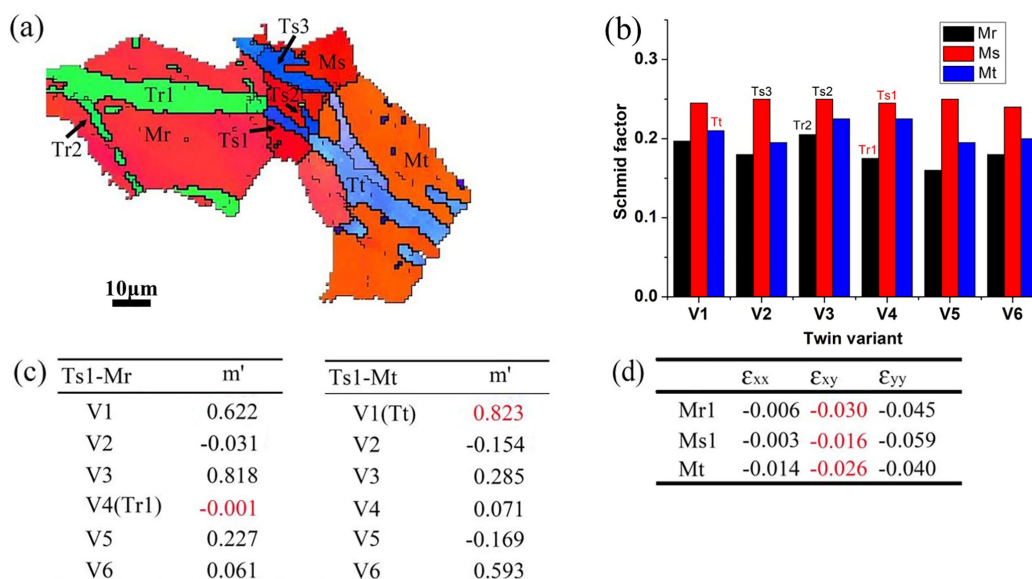


Figure 10. Analysis of twin chain across three neighboring grains, which does not follow strain compatibility factor law for region C: (a) EBSD map; (b) Schmid factor distribution figure; (c) m' distribution figure; and (d) strain tensors for twin variants.

The above observation suggests that variants with high strain compatibility may prefer activation and eventually form paired twins or twin chains to reduce stress concentration. The strain compatibility factor is more appropriate than the Schmid factor for analyzing the effect of local strain on the selection behavior of twin variants. In certain regions with non-uniform local strain, there are instances that cannot be explained by the strain compatibility factor law and Schmid factor criterion, which needs to be further investigated.

4. Conclusions

The eight-sided prism specimen was used to investigate {10-12} extension twinning during the compression of AZ31 Mg alloy. The mechanism of twin variants selection was

investigated through a comprehensive analysis of the Schmid factor and strain compatibility factor. The main conclusions can be summarized as follows:

- (1) Under inhomogeneous deformation, the strain and microstructure of the compressed AZ31 magnesium alloy sample exhibit significant variations across different regions.
- (2) Basal on SF ratio distribution, the Schmid factor criterion, can predict over 75% of observed twin variants in regions A and D (normal stress samples). In contrast, 64% of twin variant selection behavior in region C (shear stress sample) can be effectively explained using a pure shear model.
- (3) The strain compatibility factor is insensitive to the loading direction. It is more appropriate for analyzing the twin activity of twin–twin interactions in adjacent grains. In certain regions with non-uniform local strain, the twin activity is more complex and requires comprehensive evaluation.

Author Contributions: Conceptualization, B.W.; methodology, B.L. and J.Y.; formal analysis, W.W.; investigation, B.L., J.Y. and W.W.; resources, L.D.; data curation, L.X.; writing—original draft preparation, B.L. and J.Y.; writing—review and editing, L.D.; visualization, L.X.; supervision, B.W.; funding acquisition, B.W. All authors have read and agreed to the published version of the manuscript.

Funding: This work was financially supported by the Natural Science Foundation of Fujian Province of China (Grant No. 2020J01352), the Quanzhou City Science & Technology Program of China (Grant No. 2021C027R) and Collaborative Innovation Platform Project of Fu-Xia-Quan National Independent Innovation Demonstration Zone (2022-P-025).

Data Availability Statement: The original contributions presented in the study are included in the article, further inquiries can be directed to the corresponding author.

Conflicts of Interest: The authors declare no conflicts of interest.

References

1. Rahmatabadi, D.; Hashemi, R.; Tayyebi, M.; Bayati1, A. Investigation of mechanical properties, formability, and anisotropy of dual phase Mg–7Li–1Zn. *Mater. Res. Express* **2019**, *6*, 096543. [\[CrossRef\]](#)
2. Zhu, H.W.; Yu, B.Y.; Cai, J.K.; Bian, J.C.; Zheng, L. Effect of initial microstructures on microstructures and properties of extruded AZ31 alloy. *Mater. Sci. Technol.* **2023**, *39*, 1579–1591. [\[CrossRef\]](#)
3. Xie, J.L.; Zhou, Y.H.; Zhou, C.P.; Li, X.P.; Chen, Y.H. Microstructure and mechanical properties of Mg–Li alloys fabricated by wire arc additive manufacturing. *J. Mater. Res. Technol.* **2024**, *29*, 3487–3493. [\[CrossRef\]](#)
4. Zhao, X.H.; Ren, B.Q.; Zhang, Y.W.; Wang, H.; Liu, Y.; Zhang, X.E.; Chen, C. Microstructural evolution and strengthening mechanisms of CMT directed energy deposition-arc with interlayer ultrasonic impact treatment manufactured AZ31 magnesium alloy. *Mater. Sci. Eng. A-Struct. Mater. Prop. Microstruct. Process.* **2023**, *879*, 145267. [\[CrossRef\]](#)
5. Barnett, M.R. Twinning and the ductility of magnesium alloys: Part I: “Tension” twins. *Mater. Sci. Eng. A* **2007**, *464*, 1–7. [\[CrossRef\]](#)
6. Barnett, M.R. Twinning and the ductility of magnesium alloys: Part II. “Contraction” twins. *Mater. Sci. Eng. A* **2007**, *464*, 8–16. [\[CrossRef\]](#)
7. Malik, A.; Wang, Y.; Nazeer, F.; Khan, M.A.; Ali, T.; Ain, Q.T. Effect of pre-straining on twinning, texture and mechanical behavior of magnesium alloys A-review. *J. Mater. Res. Technol.* **2020**, *9*, 14478–14499. [\[CrossRef\]](#)
8. Jiang, L.; Jonas, J.J.; Mishra, R.K.; Luo, A.A.; Sachdev, A.K.; Godet, S. Twinning and texture development in two Mg alloys subjected to loading along three different strain paths. *Acta Mater.* **2007**, *55*, 3899–3910. [\[CrossRef\]](#)
9. Brown, D.W.; Almer, J.D.; Clausen, B.; Mosbrucker, P.L.; Sisneros, T.A.; Vogel, S.C. Twinning and de-twinning in beryllium during strain path changes. *Mater. Sci. Eng. A* **2013**, *559*, 29–39. [\[CrossRef\]](#)
10. Park, S.H.; Hong, S.-G.; Lee, J.H.; Huh, Y.-H. Texture evolution of rolled Mg–3Al–1Zn alloy undergoing a {10-12} twinning dominant strain path change. *J. Alloys Compd.* **2015**, *646*, 573–579. [\[CrossRef\]](#)
11. Hou, D.W.; Li, Q.Z.; Wen, H.M. Study of reversible motion of 10 $\bar{1}2$ tensile twin boundaries in a magnesium alloy during strain path changes. *Mater. Lett.* **2018**, *231*, 84–86. [\[CrossRef\]](#)
12. Wang, B.; Xin, R.; Huang, G.; Liu, Q. Effect of crystal orientation on the mechanical properties and strain hardening behavior of magnesium alloy AZ31 during uniaxial compression. *Mater. Sci. Eng. A* **2012**, *534*, 588–593. [\[CrossRef\]](#)
13. Hou, M.J.; Zhang, H.; Fan, J.F.; Zhang, Q.; Wang, L.F.; Dong, H.B.; Xu, B.S. Microstructure evolution and deformation behaviors of AZ31 Mg alloy with different grain orientation during uniaxial compression. *J. Alloys Compd.* **2018**, *741*, 514–526. [\[CrossRef\]](#)
14. Jiang, J.; Godfrey, A.; Liu, W.; Liu, Q. Microtexture evolution via deformation twinning and slip during compression of magnesium alloy AZ31. *Mater. Sci. Eng. A* **2008**, *483*, 576–579. [\[CrossRef\]](#)

15. Zhou, L.; Yan, R.; He, Z.; Wang, Z.; Wang, F.; Wei, Z.; Mao, P.; Liu, Z. Quasi-in situ observation of extension twinning of AZ31 magnesium alloy under co-directional dynamic compression. *J. Alloys Compd.* **2023**, *969*, 172495. [[CrossRef](#)]
16. Hong, S.-G.; Park, S.H.; Lee, C.S. Role of {10–12} twinning characteristics in the deformation behavior of a polycrystalline magnesium alloy. *Acta Mater.* **2010**, *58*, 5873–5885. [[CrossRef](#)]
17. Song, B.; Xin, R.; Liang, Y.; Chen, G.; Liu, Q. Twinning characteristic and variant selection in compression of a pre-side-rolled Mg alloy sheet. *Mater. Sci. Eng. A* **2014**, *614*, 106–115. [[CrossRef](#)]
18. Luo, J.R.; Godfrey, A.; Liu, W.; Liu, Q. Twinning behavior of a strongly basal textured AZ31 Mg alloy during warm rolling. *Acta Mater.* **2012**, *60*, 1986–1998. [[CrossRef](#)]
19. Barnett, M.; Keshavarz, Z.; Beer, A.; Ma, X. Non-Schmid behaviour during secondary twinning in a polycrystalline magnesium alloy. *Acta Mater.* **2008**, *56*, 5–15. [[CrossRef](#)]
20. Jonas, J.J.; Mu, S.; Al-Samman, T.; Gottstein, G.; Jiang, L.; Martin, É. The role of strain accommodation during the variant selection of primary twins in magnesium. *Acta Mater.* **2011**, *59*, 2046–2056. [[CrossRef](#)]
21. Xin, R.; Ding, C.; Guo, C.; Liu, Q. Crystallographic analysis on the activation of multiple twins in rolled AZ31 Mg alloy sheets during uniaxial and plane strain compression. *Mater. Sci. Eng. A* **2015**, *652*, 42–50. [[CrossRef](#)]
22. Lou, C.; Zhang, X.Y.; Ren, Y. Non-Schmid-based {10-12} twinning behavior in polycrystalline magnesium alloy. *Mater. Charact.* **2015**, *107*, 249–254. [[CrossRef](#)]
23. Liu, X.; Zhu, B.; Huang, G.; Li, L.; Xie, C.; Tang, C. Initiation and strain compatibility of connected extension twins in AZ31 magnesium alloy at high temperature. *Mater. Charact.* **2016**, *122*, 197–205. [[CrossRef](#)]
24. Xin, R.; Guo, C.; Xu, Z.; Liu, G.; Huang, X.; Liu, Q. Characteristics of long {10-12} twin bands in sheet rolling of a magnesium alloy. *Scr. Mater.* **2014**, *74*, 96–99. [[CrossRef](#)]
25. Shi, Z.Z. Secondary twin variant selection in Mg alloy after a strain-path change. *J. Alloys Compd.* **2017**, *696*, 510–515. [[CrossRef](#)]
26. Vasilev, E.; Knezevic, M. Experimental characterization of voids and surrounding microstructures developed under tension of Mg–Mg–3Zn, and Ti: A statistical study. *Mater. Sci. Eng. A-Struct. Mater. Prop. Microstruct. Process.* **2023**, *862*, 144411. [[CrossRef](#)]
27. Yaddanapudi, K.; Kumar, M.A.; Wang, J.; Wang, X.; Rupert, T.J.; Lavernia, E.J.; Schoenung, J.M.; Beyerlein, I.J.; Mahajan, S. Local hardening and asymmetric twin growth by twin-twin interactions in a Mg alloy. *J. Magnes. Alloys* **2023**, *11*, 176–191. [[CrossRef](#)]
28. Paramtmuni, C.; Zheng, Z.; Rainforth, W.M.; Dunne, F.P.E. Twin nucleation and variant selection in Mg alloys: An integrated crystal plasticity modelling and experimental approach. *Int. J. Plast.* **2020**, *135*, 102778. [[CrossRef](#)]
29. Guo, C.; Xin, R.; Ding, C.; Song, B.; Liu, Q. Understanding of variant selection and twin patterns in compressed Mg alloy sheets via combined analysis of Schmid factor and strain compatibility factor. *Mater. Sci. Eng. A* **2014**, *609*, 92–101. [[CrossRef](#)]
30. Shi, Z.Z.; Liu, X.F. Characteristics of cross grain boundary contraction twin pairs and bands in a deformed Mg alloy. *J. Alloys Compd.* **2017**, *692*, 274–279. [[CrossRef](#)]
31. Yoshida, Y.; Shibano, J.-I.; Ogura, M.; Saito, K.; Kajiwara, K. Localized shear deformation in magnesium alloy by four-point bending. *Mater. Sci. Eng. A-Struct. Mater. Prop. Microstruct. Process.* **2020**, *793*, 139851. [[CrossRef](#)]
32. Huang, H.T.; Godfrey, A.; Zheng, J.P.; Liu, W. Influence of local strain on twinning behavior during compression of AZ31 magnesium alloy. *Mater. Sci. Eng. A-Struct. Mater. Prop. Microstruct. Process.* **2015**, *640*, 330–337. [[CrossRef](#)]
33. Chang, Y.; Tian, J.; Deng, J.-F.; Zhou, Y.; Wang, X.; Liang, W.; Shi, Q.-X. Local twinning behavior of ZK61m magnesium alloy sheet under multiaxial stress during drawing-pressing with Erichsen test machine. *J. Alloys Compd.* **2023**, *968*, 171880. [[CrossRef](#)]
34. Fallahi, H.; Davies, C. Evolution of twinning during cyclic loading of magnesium alloy examined by quasi-in-situ EBSD. *Mater. Sci. Eng. A* **2021**, *820*, 141375. [[CrossRef](#)]
35. Jia, Y.; Jiang, S.S.; Tan, J.; Lu, Z.; Jiang, J.F.; Wang, X.J. The evolution of local stress during deformation twinning in a Mg–Gd–Y–Zn alloy. *Acta Mater.* **2022**, *222*, 117452. [[CrossRef](#)]
36. Fidler, H.; Basu, I.; DeHosson, J.T.M. Twinning induced spatial stress gradients: Local versus global stress states in hexagonal close-packed materials. *Acta Mater.* **2023**, *256*, 119142. [[CrossRef](#)]
37. Siska, F.; Drozdenko, D.; Mathis, K.; Cizek, J.; Guo, T.T.; Barnett, M. Three-dimensional crystal plasticity and HR-EBSD analysis of the local stress-strain fields induced during twin propagation and thickening in magnesium alloys. *J. Magnes. Alloys* **2023**, *11*, 657–670. [[CrossRef](#)]
38. Gao, Y.P.; Zhao, L.; Zha, M.; Du, C.F.; Hua, Z.M.; Guan, K.; Wang, H.Y. Twinning-induced plasticity with multiple twinning modes and disclinations in Mg alloys. *Int. J. Plast.* **2023**, *164*, 103595. [[CrossRef](#)]
39. Jiang, J.; Godfrey, A.; Liu, W.; Liu, Q. Identification and analysis of twinning variants during compression of a Mg–Al–Zn alloy. *Scr. Mater.* **2008**, *58*, 122–125. [[CrossRef](#)]
40. Mu, S.; Jonas, J.J.; Gottstein, G. Variant selection of primary, secondary and tertiary twins in a deformed Mg alloy. *Acta Mater.* **2012**, *60*, 2043–2053. [[CrossRef](#)]

Disclaimer/Publisher’s Note: The statements, opinions and data contained in all publications are solely those of the individual author(s) and contributor(s) and not of MDPI and/or the editor(s). MDPI and/or the editor(s) disclaim responsibility for any injury to people or property resulting from any ideas, methods, instructions or products referred to in the content.